Chemical characterization of size-selected nanoparticles emitted by a gasoline direct injection engine: Impact of a catalytic stripper

Dumitru Duca, Mostafiz Rahman, Yvain Carpentier, Claire Pirim, Adam Boies, Cristian Focsa

Chemical characterization of size-selected nanoparticles emitted by a gasoline direct injection engine: impact of a catalytic stripper

Dumitru Duca[a], Mostafiz Rahman[b,1], Yvain Carpentier[a], Claire Pirim[a], Adam Boies[b], Cristian Focsa[a,*]

[a] *University of Lille, CNRS, UMR 8523 – PhLAM – Laboratoire de Physique des Lasers Atomes et Molécules, F-59000 Lille, France*
[b] *University of Cambridge, Department of Engineering, Cambridge, CB2 1PZ, United Kingdom*

Abstract

This work combines laser desorption/ionization mass spectrometry (L2MS) and advanced statistical techniques to reveal the impact of a catalytic stripper (CS) on the chemical composition (at the molecular level) of a gasoline direct injection engine exhaust, and follow the evolution of size-dependent chemical characteristics over the whole particles size range (10–560 nm). The gas phase and polydisperse particles making up the exhaust are separated and sampled on distinct substrates using an original homebuilt two-filter system, while size-selected particles are collected using a cascade impactor and separated into 13 different size bins (smallest diameters 10–18 nm). We demonstrate that a fine molecular-level characterization of the exhaust particulate matter is necessary to assess the effect of the CS, especially for the smallest ultra-fine particles carrying the largest volatile fraction.

Keywords: Nanoparticles, Carbonaceous aerosols, Size-selective chemical characterization, Internal combustion engine, Catalytic stripper

* *Corresponding author*: Cristian Focsa, University of Lille, CNRS, UMR 8523 – PhLAM – Laboratoire de Physique des Lasers Atomes et Molécules, F-59000 Lille, France
Phone: +33 320 33 64 84, *Fax*: +33 320 33 64 63, *Email*: cristian.focsa@univ-lille.fr
[1] *Present address*: Institute for Future Transport and Cities, School of Mechanical Aerospace and Automotive Engineering, Coventry University, Coventry CV1 2JH, United Kingdom

1. Introduction

Internal combustion engine (ICE) powered vehicles constitute a major source of airborne particulate matter (PM), especially in urban areas [1, 2]. Particles emitted from vehicle engines are complex mixtures, mainly consisting of a carbonaceous core with a multitude of adsorbed compounds such as unburnt and partially oxygenated hydrocarbons, polycyclic aromatic hydrocarbons (PAHs), sulfates, and metal oxides [3, 4]. The particle's outer organic layer (the so-called surface organic fraction – SOF) exerts a considerable influence on the properties of particulate emissions (*i.e.* reactivity, toxicity, nucleation properties) and is considered a major contributor to particle-associated health hazards [5]. In this context, special attention is drawn by the ultra-fine particles (size <100 nm) due to their higher deposition fraction, deeper penetration, and higher retention rate in the lungs [6, 7]. The inhalation of these smallest particles can result in health problems beyond the lungs: the presence of combustion derived nanoparticles has been detected in the frontal cortex of autopsy brain samples [8], urine of healthy children [9], and even in the fetal side of the placenta [10]. If transported to the fetus, these particles – as carriers for potentially toxic chemical species – could significantly affect fetal health and development [10]. Most recently, a strong association between increases in PM concentration and mortality rates due to COVID-19 was evidenced [11, 12].

The automotive industry has made significant efforts to reduce the amount and impact of internal combustion engine emissions [13–15]. For this purpose, various after-treatment systems based on conversion, adsorption and trapping technologies, such as three-way catalysts, diesel oxidation catalysts, selective catalytic reduction systems and particulate matter filters have been implemented in the exhaust track of both spark and compression ignition engines [16–18]. Devices providing chemical sites for oxidation and reduction reactions (*i.e.* catalytic strippers/converters) are particularly useful as they can convert toxic by-products present in the exhaust into less hazardous substances such as carbon dioxide, water vapor, and nitrogen gas. In the meantime, recent improvements in engine technology resulted in a significant decrease in the total number and mass of PM emitted by on-road vehicles. This, however, also led to a shift in the particle diameter toward smaller sizes (lower than 100 nm [19]).

Although not a major contributor to the emitted particle mass, these ultra-fine sizes represent an important share in the total particle number (PN), which is regulated by 17 out of the 20 countries of the G-20 group (accounting for 90% of the global vehicle sales [20]). Current European Union (EU) regulations limit PN emissions for sizes above 23 nm. However, sub-23nm particles are produced in large concentrations by both Diesel and gasoline direct injection (GDI) engines [21] and can sometimes reach 30–40% of the total PN for vehicles equipped with a GDI [22]. Based on these findings, the PMP (particle measurement programme) group of the working party on pollution and energy (GRPE) of the United Nations Economic Commission for Europe (UNECE) has worked on a protocol to lower the PM 23 nm cut-off point to 10 nm [23], the PM referring only to solid (non-volatile) particles [24], *i.e.* those which do not evaporate below 350°C.

Lowering the cut-off size of measured PM might be quite challenging, as it requires more efficient aerosol conditioning technologies to remove volatile and semi-volatile compounds with minimal size-dependent particle losses and to avoid the creation of artifacts (*i.e.* particles generated in the sampling / conditioning system). Three EU Horizon 2020 projects [25–27] have worked in parallel over the past few years to propose a robust methodology and associated instrumentation (portable emissions measurement systems – PEMS) for PN measurements down to 10 nm. Recent assessment campaigns [28–30] confirmed that the developed PEMS prototypes are ready to be introduced in the future regulations. A major change proposed in the PMP draft recommendations [23] is to impose the use of a catalytic stripper (CS) as volatile particle remover (VPR) in the future 10-nm PEMS, which is considered a safer option [31] than the evaporation tube (ET) or the thermodenuder (TD). The ET, currently used in automotive particle measurement systems, is a simple and robust method when measuring particles larger than 23 nm as it is able to completely evaporate most hydrocarbons. However, this technology might lead to re-nucleation of semi-volatile species at high hydrocarbon particle concentrations and thus higher primary dilution ratios are required to reliably measure solid particles smaller than 23 nm [32, 33]. Therefore, for measuring particles in the sub-23 nm range, removing the semi-volatile aerosol fraction using a CS optimized for small losses

of ultra-fine particles can prove more efficient [34–36].

The use of CSs in emission measurement systems has been reviewed by Giechaskiel et al. [31]. Up to now, the impact of CSs on the resulting emissions has mostly been characterized physically, with comparisons between stripped and unstripped particle mass, number or size distribution. What comes into view is the current lack of information regarding its impact on the chemical composition (at the molecular level) of the emitted aerosols (with the notable exception of one study addressing marine exhaust aerosols [37]). As the chemical composition (and thus the degree of volatility) making up the SOF layer can significantly vary with engine regimes or with PM size, an extensive investigation of the physico-chemical properties of the measured objects should be undertaken to ensure the development of a PEMS instrument capable of maintaining its accuracy and reliability for a wide range of engine operating conditions (*i.e.* in real driving conditions).

In the frame of the EU Horizon 2020 PEMS4Nano project [25] we conducted extensive measurement campaigns to thoroughly analyze the physico-chemical properties of particles emitted by a single-cylinder engine in a bottom-up approach combining experimental [38] and theoretical studies [39] for the development of a PEMS prototype. The action of a home-made (University of Cambridge) CS on the measured aerosol (polydisperse and size-selected particles, gas phase) was investigated both on-line (physical characterization by an original tandem arrangement of aerodynamic aerosol classifier, differential mobility analyzer, and centrifugal particle mass analyzer [40]) and off-line (laser mass spectrometry chemical characterization of filter-collected samples). As on-line chemical characterization by aerosol mass spectrometers is limited to particles larger than ∼50nm [37], the off-line approach adopted here is the only possible solution when focusing on smaller nanoparticles (10–32 nm in the present study) of actual interest for the 10-nm PEMS development.

2. Materials and methods

2.1. Sampling

A generic single-cylinder gasoline direct injection engine was used on a test bench to generate particles with various properties for building an extensive

database through multi-technique physico-chemical characterization [38]. The engine was described in detail in a previous publication [38], only the main characteristics are briefly reminded in Table 1, Supporting Information. For the present study, two set-points were used, called in the following low speed (LS, 1200 rpm) and high speed (HS, 2000 rpm). The IMEP (indicated mean effective pressure) was kept constant at 10 bar, λ at 1.01, and the injection at 270° bTDC (before top-dead center). The engine was operating on Euro Stage V E5 Gasoline (CEC-RF-02-08 E5) with the ignition timing set for the maximum brake torque (MBT). The temperature of both coolant and oil (Agip SIGMA, 10W-40) was kept at 80°C. To ensure the cleanliness of the combustion chamber, the engine was conditioned with methane (CH_4) before changing the operating point.

Table 1: Engine specifications (b/aTDC – before/after Top Dead Center)

Specification		**Value**
Cylinder head		Pentroof type
Compression ratio		12.5:1
Bore		82 mm
Stroke		85 mm
Displacement		449 cm^3
Fuel direct injection system		Central mounted generic six-hole injector
Injection pressure		150 bars
Spark plug location		Exhaust side
Intake valve timing:	Open	334 deg. bTDC
	Close	166 deg. bTDC
Exhaust valve timing:	Open	154 deg. aTDC
	Close	330 deg. aTDC

A custom sampling line (Figure 1) was used for the simultaneous collection of engine exhaust for offline characterization and online volatile mass fraction measurements [40]. Raw engine exhaust was sampled from the exhaust pipe 10 cm downstream of the manifold. Sampled flow was then diluted using a Dekati FPS 4000 (1:30 dilution ratio) to prevent the condensation of volatile species as well as their aggregation. The main objective of this study was to assess the impact of the catalytic stripping on the gas phase, polydisperse, and size-selected particles. Two CSs were used: CS1 (1.5 l/min flow) for on-line measurements (Catalytic Instruments CS-015) and CS2 (presented in detail in reference [38]),

which was manufactured identical to CS1 by the University of Cambridge with the exception that it was adapted to accept higher flows (10 l/min) to increase the exhaust collection efficiency needed for the subsequent offline analysis. Both CSs performances in terms of hydrocarbon removal were tested to be >99% for 30 nm tetracontane ($C_{40}H_{82}$) particles at a concentration of $>10^4$ cm^{-3}. As this work focuses on the offline analysis, only the corresponding experimental details are given below, while information about the online measurement can be found in reference [40]. The upstream (unstripped) flows were analyzed/sampled using bypasses (red dashed lines in Figure 1), while the downstream (stripped) flows were collected after passing through the CS. The sampling of size-selected particles was performed with a NanoMOUDI II cascade impactor (TSI, model 125R) able to separate particles into 13 different size-bins, with nominal cut sizes of 10000, 5600, 3200, 1800, 1000, 560, 320, 180, 100, 56, 32, 18, 10 nm. The size-selected particles were deposited on aluminum foils that were cleaned and thermally treated (at 300°C) prior to the sampling to remove all possible surface contaminants. The sampling time varied between 6h and 12h. An alternative (separate) sampling of polydisperse particles and exhaust gas phase was performed with an original double-filter system recently developed in our laboratory [41]. This device is made of two quartz fiber filters (QFF) placed in series: the front filter (FF) retains the particulate matter while letting through the gas/volatile phase, which is then adsorbed by a layer of activated carbon placed on the back filter (BF). This sampling system was proven to be very efficient in separating the particulate (non-volatile) and the gas phases in combustion emissions [41]. Both front and back filters were thermally conditioned before the sampling in order to remove any possible contaminants. The sampling time was adjusted (60–80 min) in accordance with the particle concentration and size distribution in the exhaust to obtain a homogeneous layer of particles on the FF.

A total of 44 samples were collected in the two engine regimes for subsequent offline analysis. A sample labeling scheme is used in the following, indicating the engine set-point (HS or LS), the downstream (CS) or upstream sampling point, the size-bin (for size-selected particles) or the collection QFF in the double-filter device (FF for polydisperse particles, BF for gas phase). For instance,

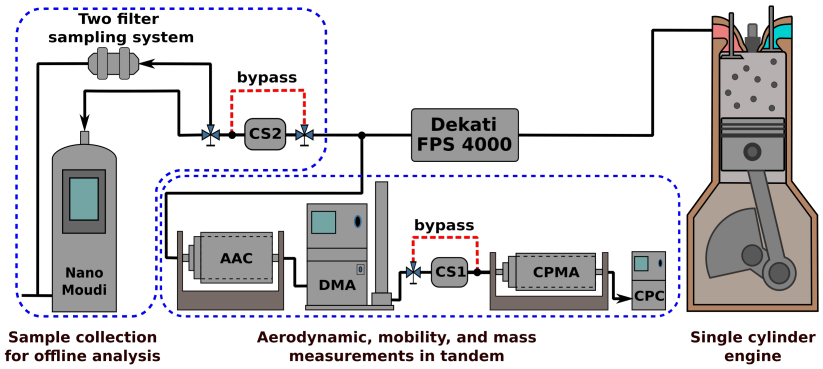

Figure 1: Schematic representation of the experimental setup. Sampling of the exhaust was conducted with a NanoMoudi II cascade impactor to size-select particles and a two-filter collection device [41] to separate the PM (polydisperse particles) and the gas phase. The collection was performed with and without the CS. The online SOF mass fraction measurements were performed with a combination of Aerodynamic Aerosol Classifier (AAC, Cambustion Ltd.), differential mobility analyzer (3080 DMA, TSI Inc.), and centrifugal particle mass analyzer (CPMA, Cambustion Ltd.) followed by a condensation particle counter (CPC, 3776, TSI Inc.) [40].

HS_CS$_{FF}$ indicates polydisperse particles collected downstream the CS in HS engine regime, while LS$_{10-18}$ labels 10–18 nm size-selected particles collected upstream the CS in the LS engine regime. In addition, a set of blank samples (aluminum foil, a neat QFF, and an activated carbon-covered QFF) were prepared, stored (at 4°C) and managed in a similar way than the collected samples.

2.2. Chemical analysis

The chemical characterization of collected particles was performed using a two-step (desorption/ionization) laser mass spectrometry technique (L2MS) described in detail elsewhere [42, 43]. The mass spectrometer used in this study (Fasmatech S&T) combines ion cooling, Radio Frequency (RF) guiding and Time-of-Flight (ToF) analyzer to reach a mass resolution of ∼15000. The sample, placed under vacuum (10^{-8} mbar residual pressure), is irradiated at 30° angle of incidence by a frequency doubled Nd:YAG laser beam (Quantel Brilliant, λ_d=532 nm, 4 ns pulse duration, 0.10–0.22 J cm^{-2} fluence, 10 Hz repetition rate) focused to a 0.07 mm^2 spot on the surface. The desorbed compounds form a gas plume that expands in the vacuum normally to the sample surface, and are ionized by an orthogonal UV laser beam (Quantel Brilliant, λ_i = 266 nm, 4 ns

pulse duration, 10 Hz repetition rate, ∼0.3 J cm^{-2} fluence). The generated ions are then RF-guided to a He collision cell for thermalization and subsequently mass analyzed in a time-of-flight mass spectrometer equipped with a reflectron (ToF-MS). The desorption and ionization fluences were adjusted for each sample to obtain the maximum signal intensity while minimizing fragmentation in the mass spectra. Each mass spectrum was obtained by averaging the signal from 200 laser shots applied on a small (∼2 mm^2) zone of the sample. To check the homogeneity of the sample surface, the analysis was performed on four different zones of each sample and all the results were used in the subsequent statistical data treatment.

Since mass spectra of the analyzed samples contain a large number of peaks its interpretation can be challenging. To optimally exploit this large amount of information, the MS data treatment follows a dedicated methodology developed in our group [44–46], which includes mass defect and multivariate analysis approaches. In this framework, a variety of advanced statistical techniques such as Principal Component Analysis (PCA) [47], Hierarchical Clustering on Principal Components (HCPC), and volcano plots [48, 49] can help uncover "hidden" patterns in complex datasets, group samples based on their similarities and identify the most significant mass peaks contributing to sample differentiation.

3. Results and discussion

3.1. Polydisperse particles and gas phase

The impact of the catalytic stripper on polydisperse PM and the gas phase was assessed by comparing the chemical composition of samples collected with and without the CS. Examples of mass spectra recorded for polydisperse particles (FF) and gas phase (BF) samples collected (in the high-speed engine regime) upstream and downstream the CS are displayed in Figure 2. The spectra contain predominantly polycyclic aromatic species and their fragments; their partial ion count (PIC) was shown to be representative of the organic carbon content of the sample [38, 46, 50]. When comparing downstream (HS_CS$_{FF}$) and upstream (HS$_{FF}$) particles, a 7-fold reduction of aromatic PIC is observed, which clearly demonstrates the efficiency of the CS in stripping the surface organic layer. Although a direct quantitative comparison is not possible (different experimental

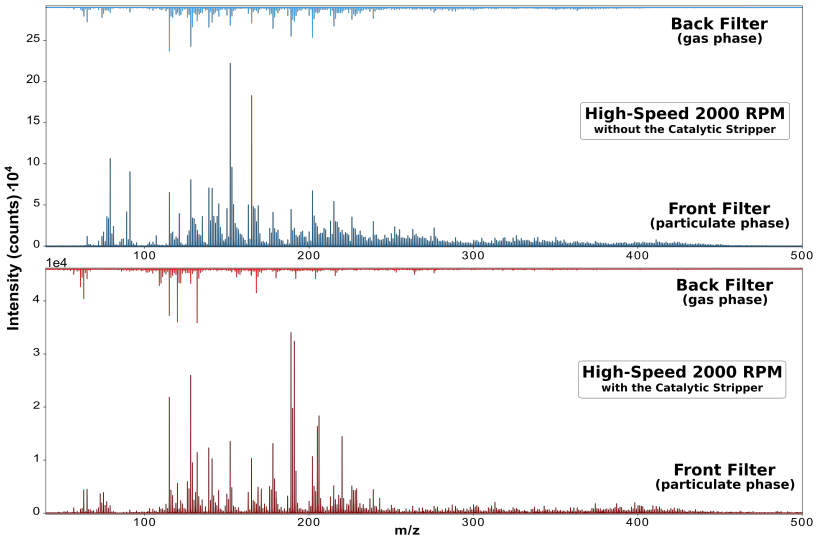

Figure 2: Mass spectra of $HS_{FF/BF}$ and $HS\_CS_{FF/BF}$ samples (particulate and gas phase collected with and without the CS) obtained with L2MS.

configurations), we note that this efficiency is in line with previous measurements performed with a soot particle aerosol mass spectrometer (SP-AMS) on marine engine exhaust, where organic species reductions in the range 94-97% were observed upon stripping [37]. The relatively small difference between the results presented here and the ones reported in Amanatidis et al. [37] might be explained by the fact that the SP-AMS instrument is only able to measure particles larger than ∼50 nm and the smallest particles below this threshold are expected to carry a higher SOF. A detailed discussion on this will be provided in the section 3.2, which focuses on size-selected particles (especially the 10–32 nm range). The efficiency of the CS in removing organics is even higher on the gas phase, as a 20-fold reduction in aromatic PIC was recorded downstream (HS_CS_{BF} sample) with respect to upstream (HS_{BF}). Indeed, the mass spectrum of the HS_CS_{BF} sample contains mostly carbon clusters (C_n^+, representative of the elemental carbon content [38, 46]) and is almost identical to the blank BF spectrum. We emphasize that the presence of carbon clusters on back filters, sampled both with and without the CS, is determined by the layer of activated carbon intended to trap the gas phase [41] and cannot be associated with the exhaust gas phase combustion by-products.

To properly interpret mass spectrometric data, mass defect analysis [44–46]

was used to assign chemical formulas to the most intense peaks. The full list of assigned peaks is provided in Table S1. A volcano plot [48, 49] was used to highlight the CS-induced changes in the chemical composition of both particulate and gas phases. The two phases carry chemical species of different volatility and mass, and thus the separate study of these phases allows to better evaluate the efficiency of the CS. The differences between the chemical composition of the particulate and gas phases can clearly be seen when the front (particulate phase) and the back filter (gas phase) sampled without the CS are compared, Figure S1. The front filter receives a high contribution from higher-mass aromatic species, with more than 4 aromatic rings. According to Bari et al. [51], the volatility of aromatic compounds can be inferred from the total number of aromatic rings: compounds consisting of only two aromatic rings are considered volatile, three to four – semi-volatile, and those with more than four aromatic rings – non-volatile. It should be noted that all the peaks corresponding to carbon clusters (C_n^+) have been excluded from this analysis since, in this case, they do not originate from the same source (soot particles for the front filters and the pre-applied black carbon layer for the back filter). However, when comparing only front filter samples (Figure 3a), carbon clusters provide important information about the variation of the OC/EC ratio (organic carbon to elemental carbon content) of sampled particles as they are commonly considered as markers of EC [46, 52–54]. Once the particles pass through the CS the contribution of aromatic compounds, considered as good indicators of the organic carbon content [38, 50], is significantly reduced, effectively decreasing the OC/EC ratio. Moreover, stripped particles feature a higher contribution from oxygenated and nitrogenated species which can be linked to the oxidation processes occurring in the CS.

A similar picture can be seen when the two samples corresponding to the gas phase (HS_{BF} and HS_CS_{BF}) are compared, Figure 3b. The gas phase sampled without the CS presents a high content of aromatic compounds (mostly low-mass, up to 4 aromatic rings), while the one collected downstream the stripper is characterized only by carbon clusters (coming from the underlying black carbon layer). The fact that no organic species contribute in a significant way to the HS_CS_{BF} mass spectrum implies that the CS removed the majority

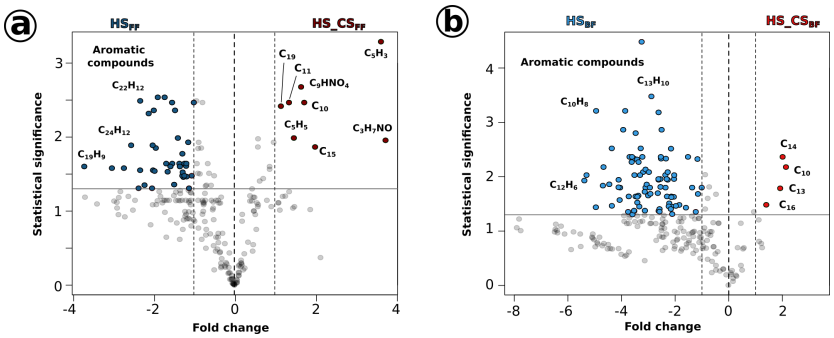

Figure 3: Volcano plots showing the "differential expression" of detected chemical species: a) comparison between the chemical composition of the particulate phase sampled with and without the CS, and b) influence of the CS on the chemical composition of the gas phase.

of combustion-generated compounds from the gas phase.

A principal component analysis of all FF and BF samples collected (with and without the CS) in both engine regimes (HS and LS) was performed. This approach allows the differentiation between samples and highlights (through the analysis of the loading plots, Figure S2) the contribution of individual compounds or groups of highly correlated species to this differentiation. The PCA was able to separate all the samples with only two principal components accounting for ∼72% of the total variance. The first principal component (∼63.9%) separates the samples based on the OC/EC ratio (a high positive PC1 score reflects a low OC/EC ratio). The volatility of the samples can be inferred from their PC2 (∼8.2% of explained variance) scores. A positive PC2 score is associated with the presence of non-volatile aromatic species (more than 4 aromatic rings) with m/z $\leq$ 363, while a negative PC2 score is linked to the presence of volatile and semi-volatile compounds, as well as some high-mass aromatic species (m/z $>$ 363). Three major regions can be seen on the score plot presented in Figure 4: i) particulate phase sampled without the CS (HS_{FF} and LS_{FF}, dark blue), ii) particulate phase sampled with the CS along with the gas phase sampled without it (HS_CS_{FF}, LS_CS_{FF} – dark red, HS_{BF}, and LS_{BF} – light blue), and iii) the gas phase collected after the CS (HS_CS_{BF} and LS_CS_{BF} - light red).

It is worth noting that even though particulate phases sampled without the stripper are located fairly close to each other and can be grouped together, their chemical composition is different. The PC1 score for the front filter (par-

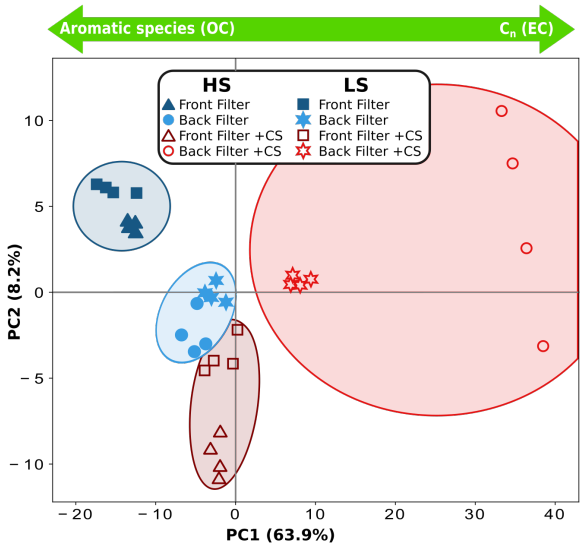

Figure 4: Score plot of the first two principal components for the particulate and gas phase samples collected with and without the CS in two different engine regimes (HS and LS). The arrows represent the meaning of the first principal component derived from the corresponding loadings plot, Figure S2.

ticulate phase) collected in the LS engine regime is lower, thus indicating a higher contribution from organic compounds in this regime. However, after the catalytic treatment, particles emitted in different engine regimes seem to have a more similar chemical composition, depicted by their almost identical PC1 scores. Moreover, the sign of the PC2 value changes after the particles have passed through the CS, suggesting the removal of the vast majority of high-mass organic compounds. The untreated gas phase contains a much smaller amount of organic species (PC1 value close to zero) which are almost completely removed by the stripper (PC1 sign changes). Therefore, mass spectra of HS_CS$_{BF}$ and LS_CS$_{BF}$ samples have a much larger contribution from the layer of activated carbon pre-applied to their surfaces, and thus the difference in PC1 value (*i.e.* contribution of elemental carbon) between the two samples cannot be attributed to combustion conditions and instead is determined by small inhomogeneities in the layer of activated carbon. The PC2 value for gas phase samples is close to zero, indicating a low influence from this component due to the insignificant number of high-mass organic species.

A volcano plot (Figure S3) was employed to compare the particulate phase

produced in the HS and LS engine regimes. When comparing unstripped particles, Figure S3a, we can see that while both samples contain a large amount of aromatic compounds, the one obtained at lower speed (LS) contains more high-mass species (*i.e.* non-volatile compounds [41, 51]). Unstripped particles collected in different regimes have a noteworthy difference in the chemical composition, demonstrated by the fact that 55 compounds contribute in a statistically significant way to their separation. In contrast, stripped particles appear to be very similar, Figure S3b. Only a few species contribute to the separation between the mass spectra of stripped particles generated in different engine regimes, and these mass spectra are mostly constituted of carbon clusters (representative of EC). This is an important result, showing that the CS is able to treat particles exhibiting quite different initial chemical composition, effectively stripping their (different) surface organic layers and leaving them as solid non-volatile PM.

3.2. Size-selected particles

Size-selected particles produced in the two engine regimes, and sampled with or without the CS were chemically characterized. For the first engine regime (HS) the stages of the cascade impactor that collected sufficient material (with and without the CS) covered a quite extended size-range: from 10 nm up to 560 nm (HS_{10-18} – $HS_{320-560}$ samples). Mass spectra of these samples are presented in Figure 5. One can see that mass spectra of particles from different size-bins are very different, indicating that the chemical composition of emitted particles significantly changes with the size. Mass spectra of particles collected without the CS show a high contribution from heavy-mass PAHs that can be associated with the remnants of the fuel or lubricating oil [38]. The majority of these compounds are successfully removed by the CS, which is illustrated by the decrease in the absolute signal intensity. At the same time the contribution of carbon clusters (C_n^+) increases, thus indicating a much lower OC/EC ratio for the stripped particles. The relative contribution of low-mass PAHs and their fragments increases toward smaller particle sizes which suggests an increase in the overall volatility of the surface organic fraction [40].

PCA was applied to the mass spectrometric data to study the impact of CS on the size dependent chemical composition. The first two principal components

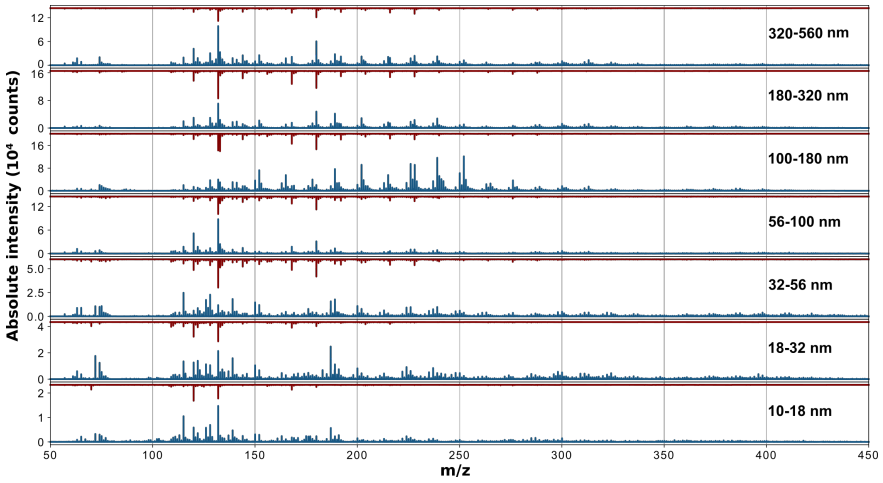

Figure 5: Mass spectra of size-selected particles produced in the HS engine regime and sampled with (red line – HS_CS) and without (blue line – HS) the catalytic stripper. The labels indicate the corresponding NanoMOUDI size-bin.

account for ∼60% of the variance in the dataset and are able to discriminate between different samples (with particles of a different size and collected with or without the catalytic stripper), Figure 6a. The meaning of each component was determined from its corresponding loadings plot, Figure S4. The first principal component (PC1) separates samples based on the contribution to mass spectra of aromatic species (OC – positive PC1 scores) and carbon clusters (C_n^+, EC – negative PC1 scores). Therefore, this component enables the discrimination between particles with a different OC/EC ratio. The HS samples have mainly positive PC1 scores while HS_CS ones – mostly negative, thus indicating that a significant amount of the organic fraction was removed from the particles by the CS. It is worth noting that the smallest analyzed particles (10–32 nm, HS_{10-18} and HS_{18-32}) are the most affected by this treatment (revealed by the large separation between $HS_{10-18,18-32}$ and $HS\_CS_{10-18,18-32}$ data points in the score plot, Figure 6a). This separation can be associated with the high relative content of organic species present on smaller particles which is almost completely removed by the CS and leading to a significant change in the PC1 score (OC/EC). Once the organic fraction is removed, the signal related to the elemental carbon (EC) becomes more important (C_n^+ ions), leading to a negative PC1 score.

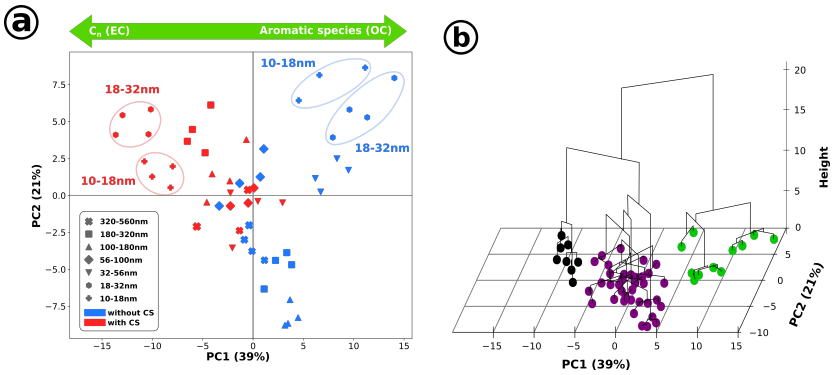

Figure 6: Impact of the CS on size-dependent PM chemical composition: a) Score plot of the first two principal components obtained from mass spectra of size-selected particles collected with (red symbols) and without (blue symbols) the CS in the HS engine regime; the arrows show the meaning of the principal components obtained from their loadings, and b) HCPC performed on the first five principal components (explaining more than 82% of the variance); three biggest clusters correspond to: small particles collected with the CS (HS_CS_{10-18} and HS_CS_{18-32}) – black markers, small particles collected without the CS (HS_{10-18}, HS_{18-32}, and HS_{32-56}) – green markers, and bigger particles collected in both regimes (HS and LS) – purple markers.

The second principal component is related to the presence of PAHs (*i.e.* stabilomers [55], negative PC2 score). Smaller particles (<100 nm) show a high contribution from fragments and PAH derivatives (positive PC2) while bigger particles (100–560 nm) contain a larger number of stabilomer PAHs that are removed by the CS (PC2 score changes from being negative to positive or almost zero). It should be noted that the spread between data points across the second dimension (PC2) is much smaller for particles collected with the CS (HS_CS), indicating that, when it comes to the organic fraction, the chemical composition of stripped size-selected particles is not very different.

HCPC was performed on the first five principal components, accounting for more than 82% of the variance within the data set, to identify the clusters that form in the principal component space and discriminate between particles, Figure 6b. Three separate clusters can be identified: small particles collected with the CS (HS_CS_{10-18} and HS_CS_{18-32}) – black markers, small particles collected without the CS (HS_{10-18}, HS_{18-32}, and HS_{32-56}) – green markers, and bigger particles collected in both regimes – red markers. This shows that the chemical composition of the smallest particles was significantly changed by the

CS, thus supporting our previous conclusion that small particles contain a high surface organic fraction which makes them more susceptible to a catalytic treatment. This conclusion is also supported by online aerodynamic-mass-mobility measurements that show that the volatile mass fraction increases for smaller particles, Figure S8.

The compounds that are efficiently removed from the smallest particles (10–18 nm) by the stripper were identified with a volcano plot, Figure S5. The CS removes the organic fraction from these particles, leading to the decrease of the OC/EC ratio. It is worth noting that, for this particular size-bin, the CS effectively removes PAHs from the entire mass-range and particles end up showing only a negligible contribution from organic species.

As the chemical composition of the emitted particles depends on the engine set-point, the CS may impact differently particles belonging to the same size-bin but generated in different engine regimes (LS or HS). To identify the (possible) change in CS efficiency, the differences between the initial (unstripped) chemical compositions of size-selected particles produced in the two engine regimes must be first identified with PCA (Figure 7a). The first two principal components account for 61% of the variation in the data set and will be used to explain the differences in the chemical composition. From the loadings plot (Figure S6a), PC1 can be linked to the contribution of PAHs (positive value), fragments, and carbon clusters (negative PC1), while PC2 can be used to separate samples based on the OC/EC ratio. For instance, samples with a low OC/EC ratio have a negative PC2 score, while the ones with a high amount of organic species exhibit a positive PC2 value. On the score plot (Figure 7a) the data points corresponding to the two engine regimes are well separated by PC1. Therefore, it is possible to distinguish between particles produced in these two regimes based only on the contribution of PAHs, fragments, and carbon clusters. PM collected in the LS engine regime features a much higher contribution from PAHs, with particles from all size-bins having a negative PC1 score (except for LS_{10-18}). In contrast, particles emitted in the HS engine regime exhibit a higher signal coming from fragments and carbon clusters. Note that the fact that HS samples show a positive PC1 score cannot be linked to a missing organic fraction and should only be seen as a lower relative contribution of the peaks attributed

to organic species compared to that observed for LS samples. PC2 shows that in the LS regime, the smallest particles yield the highest OC/EC ratio, also higher than that of the corresponding HS sample. The biggest particles (56–560 nm) produced in the HS regime show the highest contribution from carbon clusters, *i.e.* the lowest OC/EC. In addition, smaller particles from the HS regime (10–100 nm) show the highest partition of organic species. Particles in the size range of 100–320 nm produced in both regimes display a similar PC2 score, implying that they are the least affected by the change in engine operating conditions.

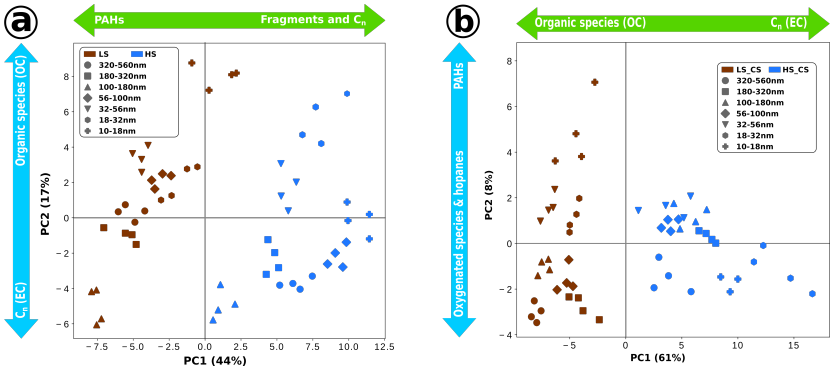

Figure 7: Score plot of the first two principal components obtained from the mass spectra of size-selected particles collected in the LS and HS engine regimes without (a) and with (b) the catalytic stripper. The arrows indicate the meaning of principal components obtained from their corresponding loadings.

Once the differences between the chemical compositions of unstripped particles produced in the two engine regimes have been identified, the effect of the CS on size-selected PM with different chemical composition can be determined by PCA, as shown in Figure 7b. The first two principal components explain 69% of the observed variance and are able to distinguish between stripped particles generated in the two engine regimes based on the few chemical species left on the surface. The first principal component (61%) groups samples based on their OC/EC ratio, determined from the corresponding loadings plot (Figure S6b). It should be noted that PCA is emphasizing the variance in the dataset, and thus the separation between particles observed on the score plot (Figure 7b) cannot be used to quantify, for instance, the difference in the organic content. The majority of organic species present on raw particles are successfully stripped by the CS, making their chemical composition comparable, similar to what was shown

before for polydisperse particles. However, the high sensitivity of the analytical technique [43] used here reveals distinct features in size-selected stripped particles collected in different engine regimes. For instance, when comparing the smallest treated particles (10–18 nm) collected in different engine regimes with a volcano plot (Figure S7) we can see that only a few species contribute to the separation between the samples. Due to their small mass, the chemical information related to these particles is usually lost when polydisperse PM is collected, thus illustrating the importance of size-selective analysis. The spread between data points on the PC1 axis is rather small, suggesting that stripped particles of different sizes have a comparable amount of OC.

The second principal component is linked to the amount of aromatic species (positive PC2 score), oxygenated, and hopanoid compounds (negative PC2 score). The latter group of compounds is often used as marker species for remnants of lubricating oil [38]. The CS successfully removes these compounds from particles smaller than 100 nm, however, bigger LS_CS particles (100–560 nm) still contain residues of these compounds. Even though particles in three size-bins sampled in the HS_CS engine regime ($HS\_CS_{320-560}$, HS_CS_{18-32}, HS_CS_{10-18}) also show a negative PC2 score, they do not exhibit a high hopanoid content but are instead characterized by a higher content of oxygenated species (identified from volcano plots). The HS_CS cluster is located very close to the PC2 axis, suggesting, once again, their lower OC/EC ratio compared to LS_CS particles.

4. Conclusions

To the best of our knowledge, this is the first study to tackle a detailed, molecular-level characterization of the impact of a CS (in a PEMS context) on the chemical composition of an ICE exhaust. Most of the studies test the CS removal efficiency on tetracontane ($C_{40}H_{82}$) particles, following the recommendations of the PMP protocol [20]. Amanatidis et al. [35] used liquid decane ($C_{10}H_{22}$) and toluene (C_7H_8) injected in a 10% v/v O_2 in N_2 gas mixture to measure efficiencies >90% for the removal of these hydrocarbons by a CS, while preliminary tests with a heavier (C_{16}) species led to artifacts and inconclusive results. In another study, Amanatidis et al. [37] measured stripping efficiencies

of organics in the range 94-97% from particles (>50 nm) emitted by a marine engine. The results of the present study on polydisperse particles and gas phase emitted by a single-cylinder GDI are well in line with those previous findings and foster the use of a CS-based VPR system in future PEMS.

A specificity of our work is the study of the chemical composition of particles selected by size. Indeed, the composition of engine exhaust PM can significantly change not only with the engine set-point but also with the particle size [38]. When polydisperse PM is studied, a weighted average composition of particles of various sizes is obtained, with individual weights related to the initial particle size distribution which can significantly change depending on the engine set-point. This is clearly illustrated here by analyzing PM emitted in two engine operation regimes. The fine statistical analysis of the CS action on size-selected particles revealed (despite the high removal efficiency) the "memory" of the initial (unstripped) composition of the particles, which was not possible with the polydisperse PM. This further stresses how important it is to sample and characterize size-selected particulate matter, especially since the chemical composition of the smallest particles (with low contribution to the total mass in a polydisperse sample) cannot be otherwise inferred. Deposition on filters/substrates and offline analysis seems to be the only option here, as aerosol mass spectrometers are typically limited to sizes above ∼50 nm.

This work also showed that the smallest particles (10–32 nm) are the most affected by the CS, indicating that particles in this size range carry a larger volatile fraction. This conclusion concurs with the results of online aerodynamic-mass-mobility tandem measurements [40] performed in parallel with the collection of samples described here: on-line (physical) and off-line (chemical) investigations are in excellent agreement. The online measurements revealed an increasing contribution of the particle-bound volatile mass fraction toward smaller particles sizes, as illustrated in Figure S8. The excellent agreement between these two completely independent (chemical and physical) characterization methods demonstrates the reliability of the used experimental approaches and validates the main conclusions of the study, which is also supported by theoretical investigations [39] conducted in the PEMS4Nano project and showing the same trend of the SOF with size. Moreover, the obtained trend also matches previous

dynamometer and on-road testing showing that semi-volatile particles represent a significant fraction of the smallest nanoparticles [56, 57].

We demonstrated that a fine molecular-level characterization of the exhaust PM is necessary to precisely evaluate the effect of a CS, especially for the smallest ultra-fine particles. As the particles' outer organic layer consists of a multitude of chemical species (*e.g.* PAHs) and that the smallest particles tend to exhibit a larger volatile fraction, the ultra-fine PM could present a double risk – due to their small size they penetrate deeper in the respiratory system while also carrying a larger amount of potentially toxic compounds. This not only shows how important is the addition of oxidation catalysts in after-treatment systems of modern vehicles to remove the (potentially toxic) organic fraction from the engine exhaust, but also how crucial is the regulation of the small sub-23 nm particles.

Acknowledgments

This study has received funding as a part of the PEMS4Nano project from the European Union's Horizon 2020 research and innovation programme under Grant Agreement No. 724145. Additionally, this work was supported by the French National Research Agency (ANR) under contract ANR-18-CE22-0019 (UNREAL) and through the PIA (Programme d'Investissement d'Avenir) under contract ANR-10-LABX-005 (LABEX CaPPA - Chemical and Physical Properties of the Atmosphere) and by the UK EPSRC Centre for Sustainable Road Freight (EP/R035199/1) and NERC Integrated Research Observation System for Clean Air (NE/T001909/1).

References

[1] C. Guerreiro, A. Ortiz, F. de Leeuw, M. Viana, Air quality 2018 - EEA report 12 2018, Publications Office of the European Union, 2018. doi:10.2800/777411.

[2] F. Karagulian, C. A. Belis, C. F. C. Dora, A. M. Prüss-Ustün, S. Bonjour, H. Adair-Rohani, M. Amann, Contributions to cities' ambient particulate matter (pm): A systematic review of local source contributions

at global level, Atmospheric Environment 120 (2015) 475–483. doi:10.1016/j.atmosenv.2015.08.087.

[3] J. H. Johnson, S. T. Bagley, L. D. Gradz, D. G. Leddy, A review of diesel particulate control technology and emissions effects, Horning Memorial Award Lecture SAE paper 940233 (1994). doi:10.4271/940233.

[4] B. R. Stanmore, J. F. Brilhac, P. Gilot, The oxidation of soot: a review of experiments, mechanisms and models, Carbon 39 (2001) 2247–2268. doi:10.1016/S0008-6223(01)00109-9.

[5] Z. D. Ristovski, B. Miljevic, N. C. Surawski, L. Morawska, K. M. Fong, F. Goh, I. A. Yang, Respiratory health effects of diesel particulate matter, Respirology 17 (2012) 201–212. doi:10.1111/j.1440-1843.2011.02109.x.

[6] H.-S. Kwon, M. H. Ryu, C. Carlsten, Ultrafine particles: unique physicochemical properties relevant to health and disease, Experimental & Molecular Medicine 52 (2020) 318–328. doi:10.1038/s12276-020-0405-1.

[7] Y. Li, K. J. Lane, L. Corlin, A. P. Patton, J. L. Durant, M. Thanikachalam, M. Woodin, M. Wang, D. Brugge, Association of long-term near-highway exposure to ultrafine particles with cardiovascular diseases, diabetes and hypertension, International journal of environmental research and public health 14 (2017) 461–477. doi:10.3390/ijerph14050461.

[8] B. A. Maher, I. A. Ahmed, V. Karloukovski, D. A. MacLaren, P. G. Foulds, D. Allsop, D. M. Mann, R. Torres-Jardón, L. Calderon-Garciduenas, Magnetite pollution nanoparticles in the human brain, Proceedings of the National Academy of Sciences 113 (2016) 10797–10801. doi:10.1073/pnas.1605941113.

[9] N. D. Saenen, H. Bové, C. Steuwe, M. B. Roeffaers, E. B. Provost, W. Lefebvre, C. Vanpoucke, M. Ameloot, T. S. Nawrot, Children's urinary environmental carbon load. a novel marker reflecting residential ambient air pollution exposure?, American Journal of Respiratory and Critical Care Medicine 196 (2017) 873–881. doi:10.1164/rccm.201704-0797OC.

[10] H. Bové, E. Bongaerts, E. Slenders, E. M. Bijnens, N. D. Saenen, W. Gyselaers, P. Van Eyken, M. Plusquin, M. B. Roeffaers, M. Ameloot, et al., Ambient black carbon particles reach the fetal side of human placenta, Nature communications 10 (2019) 3866. doi:10.1038/s41467-019-11654-3.

[11] L. Setti, F. Passarini, G. De Gennaro, P. Barbieri, A. Pallavicini, M. Ruscio, P. Piscitelli, A. Colao, A. Miani, Searching for SARS-COV-2 on particulate matter: A possible early indicator of COVID-19 epidemic recurrence, International Journal of Environmental Research and Public Health 17 (2020) 2986–2991. doi:10.3390/ijerph17092986.

[12] D. Contini, F. Costabile, Does air pollution influence COVID-19 outbreaks?, Atmosphere 11 (2020) 377–382. doi:10.3390/atmos11040377.

[13] H. C. Frey, Trends in onroad transportation energy and emissions, Journal of the Air and Waste Management Association 68 (2018) 514–563. doi:10.1080/10962247.2018.1454357.

[14] P. Bielaczyc, J. Woodburn, Trends in automotive emission legislation: impact on ld engine development, fuels, lubricants and test methods: a global view, with a focus on wltp and rde regulations, Emission Control Science and Technology 5 (2019) 86–98. doi:10.1007/s40825-019-0112-3.

[15] B. Giechaskiel, A. Joshi, L. Ntziachristos, P. Dilara, European regulatory framework and particulate matter emissions of gasoline light-duty vehicles: A review, Catalysts 9 (2019) 586. doi:10.3390/catal9070586.

[16] G. C. Koltsakis, A. M. Stamatelos, Catalytic automotive exhaust aftertreatment, Progress in Energy and Combustion Science 23 (1997) 1–39. doi:10.1016/S0360-1285(97)00003-8.

[17] E. Meloni, V. Palma, Most recent advances in diesel engine catalytic soot abatement: Structured catalysts and alternative approaches, Catalysts 10 (2020) 745. doi:10.3390/catal10070745.

[18] A. Mamakos, M. Schwelberger, M. Fierz, B. Giechaskiel, Effect of selective catalytic reduction on exhaust nonvolatile particle emissions of euro vi

heavy-duty compression ignition vehicles, Aerosol Science and Technology 53 (2019) 898–910. doi:10.1080/02786826.2019.1610153.

[19] P. Karjalainen, L. Pirjola, J. Heikkilä, T. Lähde, T. Tzamkiozis, L. Ntziachristos, J. Keskinen, T. Rönkkö, Exhaust particles of modern gasoline vehicles: A laboratory and an on-road study, Atmospheric Environment 97 (2014) 262–270. doi:10.1016/j.atmosenv.2014.08.025.

[20] M. Williams, R. Minjares, A technical summary of euro 6/vi vehicle emission standards. icct (international council on clean transportation) briefing (2016).
URL https://theicct.org/publications/technical-summary-euro-6vi-vehicle-emissionstandards

[21] B. Giechaskiel, U. Manfredi, G. Martini, Engine exhaust solid sub-23 nm particles: I. literature survey, SAE International Journal of Fuels and Lubricants 7 (2014) 950–964. doi:10.4271/2014-01-2834.

[22] B. Giechaskiel, J. Vanhanen, M. Vakeva, G. Martini, Investigation of vehicle exhaust sub-23 nm particle emissions, Aerosol Science and Technology 51 (2017) 626–641. doi:10.4271/2014-01-2834.

[23] G. Martini, T. Grigoratos, PMP IWG Progress Report; 81st UNECE GRPE session, 9–11 June 2020 (2020).
URL http://www.unece.org/fileadmin/DAM/trans/doc/2020/wp29grpe/GRPE-81-31e.pdf

[24] B. Giechaskiel, E. Schiefer, W. Schindler, H. Axmann, C. Dardiotis, Overview of soot emission measurements instrumentation: From smoke and filter mass to particle number, SAE International Journal of Engines 6 (2013) 10–22. doi:10.4271/2013-01-0138.

[25] PEMs4Nano. European Union's Horizon 2020 research and innovation programme under grant agreement Nr. 724145, accessed on 17 August 2020 (2020).
URL https://pems4nano.eu

[26] DownToTen. European Union's Horizon 2020 research and innovation progamme under grant agreement Nr. 724085, accessed on 17 August 2020 (2020).
URL https://downtoten.com

[27] SUREAL-23. European Union's Horizon 2020 research and innovation progamme under grant agreement Nr. 724136, accessed on 17 August 2020 (2020).
URL http://sureal-23.cperi.certh.gr

[28] B. Giechaskiel, A. Mamakos, J. Woodburn, A. Szczotka, P. Bielaczyc, Evaluation of a 10 nm particle number portable emissions measurement system (PEMS), Sensors 19 (2019) 5531. doi:10.3390/s19245531.

[29] B. Giechaskiel, P. Bonnel, A. Perujo, P. Dilara, Solid particle number (SPN) portable emissions measurement systems (PEMS) in the European legislation: A review, International Journal of Environmental Research and Public Health 16 (2019) 4819. doi:10.3390/ijerph16234819.

[30] B. Giechaskiel, T. Lähde, S. Gandi, S. Keller, P. Kreutziger, A. Mamakos, Assessment of 10-nm Particle Number (PN) Portable Emissions Measurement Systems (PEMS) for Future Regulations, International Journal of Environmental Research and Public Health 17 (2020) 3878. doi:10.3390/ijerph17113878.

[31] B. Giechaskiel, A. D. Melas, T. Lähde, G. Martini, Non-Volatile Particle Number Emission Measurements with Catalytic Strippers: A Review, Vehicles 2 (2020) 342–364. doi:10.3390/vehicles2020019.

[32] B. Giechaskiel, Y. Drossinos, Theoretical investigation of volatile removal efficiency of particle number measurement systems, SAE International Journal of Engines 3 (2010) 1140–1151. doi:10.4271/2010-01-1304.

[33] H. Yamada, K. Funato, H. Sakurai, Application of the PMP methodology to the measurement of sub-23 nm solid particles: calibration procedures, experimental uncertainties, and data correction methods, Journal of Aerosol Science 88 (2015) 58–71. doi:10.1016/j.jaerosci.2015.06.002.

[34] A. Melas, V. Koidi, D. Deloglou, E. Daskalos, D. Zarvalis, E. Papaioannou, A. Konstandopoulos, Development and evaluation of a catalytic stripper for the measurement of solid ultrafine particle emissions from internal combustion engines, Aerosol Science and Technology 54 (2020) 704–717. doi:10.1080/02786826.2020.1718061.

[35] S. Amanatidis, L. Ntziachristos, B. Giechaskiel, D. Katsaounis, Z. Samaras, A. Bergmann, Evaluation of an oxidation catalyst ("catalytic stripper") in eliminating volatile material from combustion aerosol, Journal of aerosol science 57 (2013) 144–155. doi:10.1016/j.jaerosci.2012.12.001.

[36] L. Ntziachristos, S. Amanatidis, Z. Samaras, B. Giechaskiel, A. Bergmann, Use of a catalytic stripper as an alternative to the original PMP measurement protocol, SAE International Journal of Fuels and Lubricants 6 (2013) 532–541. doi:10.4271/2013-01-1563.

[37] S. Amanatidis, L. Ntziachristos, P. Karjalainen, E. Saukko, P. Simonen, N. Kuittinen, P. Aakko-Saksa, H. Timonen, T. Rönkkö, J. Keskinen, Comparative performance of a thermal denuder and a catalytic stripper in sampling laboratory and marine exhaust aerosols, Aerosol Science and Technology 52 (2018) 420–432. doi:10.1080/02786826.2017.1422236.

[38] C. Focsa, D. Duca, J. A. Noble, M. Vojkovic, Y. Carpentier, C. Pirim, C. Betrancourt, P. Desgroux, T. Trischer, J. Spielvogel, M. Rahman, A. Boies, K. F. Lee, A. N. Bhave, S. Legendre, O. Lancry, P. Kreutziger, M. Rieker, Multi-technique physico-chemical characterization of particles generated by a gasoline engine: towards measuring tailpipe emissions below 23 nm, Atmospheric Environment 235 (2020) 117642. doi:10.1016/j.atmosenv.2020.117642.

[39] K. F. K. Lee, N. Eaves, S. Mosbach, D. Ooi, J. Lai, A. Bhave, A. Manz, J. N. J. Geiler, J. A. J. Noble, D. Duca, C. Focsa, J. Niklas, G. Robert, B. Gmbh, J. A. J. Noble, D. Duca, Model Guided Application for Investigating Particle Number (PN) Emissions in GDI Spark Ignition Engines, SAE International Journal of Advances and Current Practices in Mobility-V128-99EJ 26 (2019) 76–88. doi:10.4271/2019-26-0062.

[40] M. Kazemimanesh, M. Rahman, D. Duca, T. Johnson, A. Addad, G. Giannopoulos, C. Focsa, A. Boies, Morphology and volatility of particulate emissions from gasoline direct injection engine using aerodynamic diameter, mobility diameter, and mass measurements in tandem, submitted to Aerosol Science and Technology (2020).

[41] L. D. Ngo, D. Duca, J. A. Noble, A. R. Ikhenazene, M. Vojkovic, Y. Carpentier, C. Irimiea, Chemical discrimination of the particulate and gas phases of miniCAST exhausts using a two-filter collection method, Atmospheric Measurement Techniques 13 (2020) 951–967. doi:10.5194/amt-13-951-2020.

[42] A. Faccinetto, P. Desgroux, M. Ziskind, E. Therssen, C. Focsa, High-sensitivity detection of polycyclic aromatic hydrocarbons adsorbed onto soot particles using laser desorption/laser ionization/time-of-flight mass spectrometry: An approach to studying the soot inception process in low-pressure flames, Combustion and Flame 158 (2011) 227–239. doi:10.1016/j.combustflame.2010.08.012.

[43] A. Faccinetto, C. Focsa, P. Desgroux, M. Ziskind, Progress toward the Quantitative Analysis of PAHs Adsorbed on Soot by Laser Desorption/Laser Ionization/Time-of-Flight Mass Spectrometry, Environmental Science and Technology 49 (2015) 10510–10520. doi:10.1021/acs.est.5b02703.

[44] C. Irimiea, A. Faccinetto, Y. Carpentier, I. K. Ortega, N. Nuns, E. Therssen, P. Desgroux, C. Focsa, A comprehensive protocol for chemical analysis of flame combustion emissions by secondary ion mass spectrometry, Rapid Communications in Mass Spectrometry 32 (2018) 1015–1025. doi:10.1002/rcm.8133.

[45] C. Irimiea, A. Faccinetto, X. Mercier, I.-K. Ortega, N. Nuns, E. Therssen, P. Desgroux, C. Focsa, Unveiling trends in soot nucleation and growth: When secondary ion mass spectrometry meets statistical analysis, Carbon 144 (2019) 815–830. doi:10.1016/j.carbon.2018.12.015.

[46] D. Duca, C. Irimiea, A. Faccinetto, J. A. Noble, M. Vojkovic, Y. Carpentier,

I. K. Ortega, C. Pirim, C. Focsa, On the benefits of using multivariate analysis in mass spectrometric studies of combustion-generated aerosols, Faraday Discussions 218 (2019) 115–137. doi:10.1039/C8FD00238J.

[47] T. Adam, R. R. Baker, R. Zimmermann, Characterization of puff-by-puff resolved cigarette mainstream smoke by single photon ionization-time-of-flight mass spectrometry and principal component analysis, Journal of Agricultural and Food Chemistry 55 (2007) 2055–2061. doi:10.1021/jf062360x.

[48] W. Li, Volcano plots in analyzing differential expressions with mRNA microarrays, Journal of Bioinformatics and Computational Biology 10 (2012) 1231003. doi:10.1142/S0219720012310038.

[49] L. Shi, W. Tong, H. Fang, U. Scherf, J. Han, R. K. Puri, F. W. Frueh, F. M. Goodsaid, L. Guo, Z. Su, T. Han, J. C. Fuscoe, Z. A. Xu, T. A. Patterson, H. Hong, Q. Xie, R. G. Perkins, J. J. Chen, D. A. Casciano, Cross-platform comparability of microarray technology: Intra-platform consistency and appropriate data analysis procedures are essential, BMC Bioinformatics 6 (2005) S12–S26. doi:10.1186/1471-2105-6-S2-S12.

[50] D. Delhaye, F. X. Ouf, D. Ferry, I. K. Ortega, O. Penanhoat, S. Peillon, F. Salm, X. Vancassel, C. Focsa, C. Irimiea, N. Harivel, B. Perez, E. Quinton, J. Yon, D. Gaffie, The MERMOSE project: Characterization of particulate matter emissions of a commercial aircraft engine, Journal of Aerosol Science 105 (2017) 48–63. doi:10.1016/j.jaerosci.2016.11.018.

[51] M. A. Bari, G. Baumbach, B. Kuch, G. Scheffknecht, Particle-phase concentrations of polycyclic aromatic hydrocarbons in ambient air of rural residential areas in southern Germany, Air Quality, Atmosphere and Health 3 (2010) 103–116. doi:10.1007/s11869-009-0057-8.

[52] T. Ferge, E. Karg, A. Schröppel, K. R. Coffee, H. J. Tobias, M. Frank, E. E. Gard, R. Zimmermann, Fast determination of the relative elemental and organic carbon content of aerosol samples by on-line single-particle aerosol time-of-flight mass spectrometry, Environmental Science and Technology 40 (10) (2006) 3327–3335. doi:10.1021/es050799k.

[53] J. Pagels, D. D. Dutcher, M. R. Stolzenburg, P. H. Mcmurry, M. E. Gälli, D. S. Gross, Fine-particle emissions from solid biofuel combustion studied with single-particle mass spectrometry: Identification of markers for organics, soot, and ash components, Journal of Geophysical Research Atmospheres 118 (2013) 859–870. doi:10.1029/2012JD018389.

[54] O. B. Popovicheva, C. Irimiea, Y. Carpentier, I. K. Ortega, E. D. Kireeva, N. K. Shonija, J. Schwarz, M. Vojtíšek-Lom, C. Focsa, Chemical composition of diesel/biodiesel particulate exhaust by FTIR spectroscopy and mass spectrometry: Impact of fuel and driving cycle, Aerosol and Air Quality Research 17 (2017) 1717–1734. doi:10.4209/aaqr.2017.04.0127.

[55] S. E. Stein, A. Fahr, High-temperature stabilities of hydrocarbons, Journal of Physical Chemistry 89 (1985) 3714–3725. doi:10.1021/j100263a027.

[56] J. Ko, K. Kim, W. Chung, C. L. Myung, S. Park, Characteristics of on-road particle number (PN) emissions from a GDI vehicle depending on a catalytic stripper (CS) and a metal-foam gasoline particulate filter (GPF), Fuel 238 (2019) 363–374. doi:10.1016/j.fuel.2018.10.091.

[57] A. Momenimovahed, D. Handford, M. D. Checkel, J. S. Olfert, Particle number emission factors and volatile fraction of particles emitted from on-road gasoline direct injection passenger vehicles, Atmospheric Environment 102 (2015) 105–111. doi:10.1016/j.atmosenv.2014.11.045.